C h a p t e r 2

BRUSH POLYMER APPLICATIONS: PHOTONIC CRYSTALS

Reproduced in part with permission from:
Sveinbjörnsson, B. R.; Weitekamp, R. A.; Miyake, G. M.; Xia, Y.; Atwater, H. A.; Grubbs, R. H. *Proc. Natl. Acad. Sci. U.S.A.* **2012**, *109*, 14332-14336.

ABSTRACT

This chapter describes a study on the self-assembly of brush block copolymers into photonic crystals. The reduced chain entanglement of brush polymers over their linear analogs drastically lowers the energetic barriers to reorganization. Herein, the rapid self-assembly of brush block copolymers to nanostructures with photonic bandgaps spanning the entire visible spectrum, from ultraviolet (UV) to near infrared (NIR), is demonstrated. Linear relationships were observed between the peak wavelengths of reflection and polymer molecular weights. This work enables "bottom-up" fabrication of photonic crystals with application-tailored bandgaps through synthetic control of the polymer molecular weight and the method of self-assembly. These polymers could be developed into NIR-reflective paints to combat the "urban heat island effect" due to NIR photon thermalization.

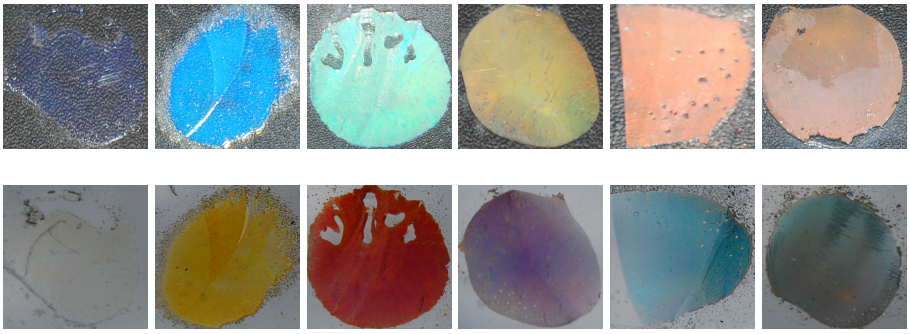

INTRODUCTION

The self-assembly of block copolymers (BCPs) into a variety of morphologies,[1–4] as well as their potential to selectively incorporate additives,[5] has earned them increased interest for many applications, including construction of photonic crystals. Photonic crystals are materials with periodic structures of different refractive indices, resulting in reflection of specific ranges of electromagnetic waves, thus creating a photonic band gap.[6,7] In order to tune these materials for specific purposes, such as for optical materials, telecommunications, and in the energy field, it is important to be able to control the range of the light these materials reflect. IR-reflecting materials are of special appeal for energy conservation purposes, since there is a substantial amount of thermal energy in IR light and these materials could therefore be used, e.g. in window coatings to reduce energy costs.[8–10] Photonic crystals are also seen in nature, contributing to the colors of butterfly wings, bird feathers, and opals.[6] The ability to synthetically mimic these properties is therefore of fundamental interest.

Despite their desirability, critical challenges must be addressed before BCPs can be broadly utilized as photonic crystals. Obtaining BCPs with the large domain sizes required to reflect the wavelengths of interest is a critical limitation.[9,11,12] The high molecular weights required make the synthesis of these polymers difficult, and chain entanglement also retards the self-assembly process. To the best of our knowledge, the self-assembly of linear BCPs has not yet been used successfully to form photonic crystals that can reach far into the visible spectra without the need for additional techniques, such as swelling the material with additives, including small molecules, inorganic nanoparticles, or other polymers.[5,8,9,12–14] While other approaches, such as layer-by-layer stacking,[15,16] electrochemical etching,[17,18] laser-beam-scanning chemical vapor deposition,[19] holographic lithography,[20,21] and self-assembly of monodisperse colloidal particles,[22,23] have been used successfully to yield well-defined photonic crystals, these methods often require expensive apparatus and complex processes.

However, brush polymers have recently shown potency as a platform material for photonic crystals. High molecular weight brush BCPs have been shown to self-assemble into domain sizes of over 100 nm,[24–28] as well as self-assembling into photonic material reflecting blue and even green light.[25,27,28] The steric crowding of the side chains forces the main chain to be in an extended conformation, yielding cylindrical structures.[29] Brush polymers also show less entanglement

compared to their linear analogs, resulting in rapid self-assembly.[28,30] In this chapter, we describe a successful approach to synthesizing brush BCPs, and fabricate them in a simple manner into an array of well-controlled photonic crystals that reflect wavelengths into the NIR region.

RESULTS AND DISCUSSION

In order to find a convenient model system to work with, a variety of different macromonomer (MM) systems were tested to observe roughly what degrees of polymerizations would be required for the brush BCPs to reflect light in the visible region. All the polymers used were based on MMs with a norbornene (NB) backbone that was polymerized via ring-opening metathesis polymerization (ROMP) using a ruthenium-based catalyst (**Figure 2-1**). The side chains of the different systems used were (1) polylactide (PLA) ($M_w \approx 4.4 \times 10^3$ g/mol) and a dodecanyl group (C12), (2) PLA ($M_w \approx 4.4 \times 10^3$ g/mol) and a "wedge" side chain, (3) poly *tert*-butyl acrylate (P*t*BA) and polystyrene (PS) side chains ($M_w \approx 5.1 \times 10^3$ g/mol), and (4) PLA ($M_w \approx 4.4 \times 10^3$ g/mol) and PS side chains ($M_w \approx 5.1 \times 10^3$ g/mol).

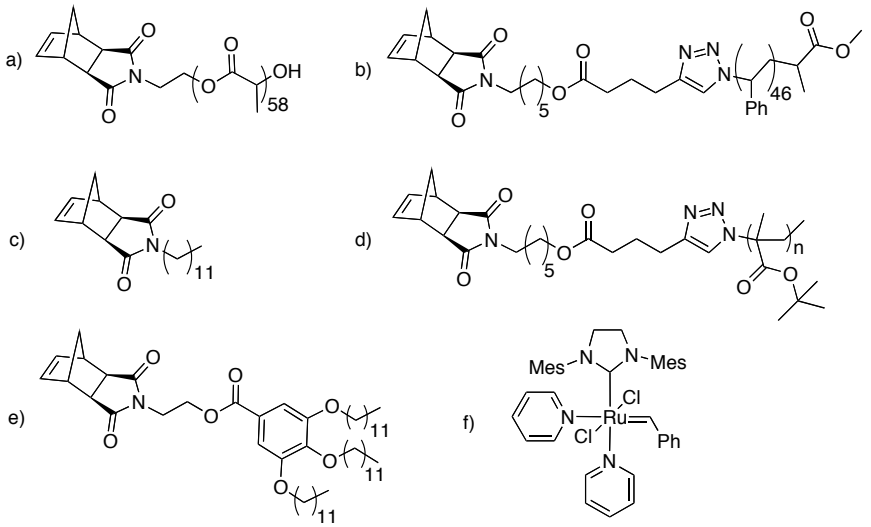

Figure 2-1. Chemical structure of the macromonomers tested and the catalyst used: a) Norbornene-polylactide (NB-PLA), b) norbornene-polystyrene (NB-PS), c) dodecanyl norbornene (NB-C12), d) norbornene *tert*-butyl acrylate (NB-*t*BA), e) norbornene wedge (NB-wedge), and f) ruthenium based metathesis catalyst used in ring-opening metathesis polymerizations.

The different combinations of MMs were copolymerized in various ratios, mainly asymmetrical, but in the case of the NB-tPBA/NB-PS as well as the NB-PLA/NB-PS copolymerizations, the MMs were also copolymerized in symmetrical ratios (**Table 2-1**).

Table 2-1. Preliminary tests of several combinations of macromonomers.

Test #	Side chain A	Side chain B	A:B:catalyst ratio	Observed color
1	PLA	C12	200:1000:1	Dark blue
2	PLA	C12	200:1500:1	Light blue
3	PLA	C12	200:2000:1	-
4	PLA	Wedge	200:1000:1	Blue
5	PLA	Wedge	200:2000:1	Green
6	PLA	PS	400:200:1	Dark blue
7	PLA	PS	400:400:1	Green
8	PtBA	PS	400:400:1	-

After the ROMP, the samples were purified, dried, and isolated as white solids. Then they were annealed by controlled evaporation from tetrahydrofuran (THF) or dichloromethane (DCM) to yield colored films. In most of the cases the color was easily observed (**Figure 2-2**), but the copolymerization of PLA and PS, which reached green color when polymerized at a ratio of 400:400:1 (PLA:PS:catalyst), was deemed the most convenient system to use for a more detailed study.

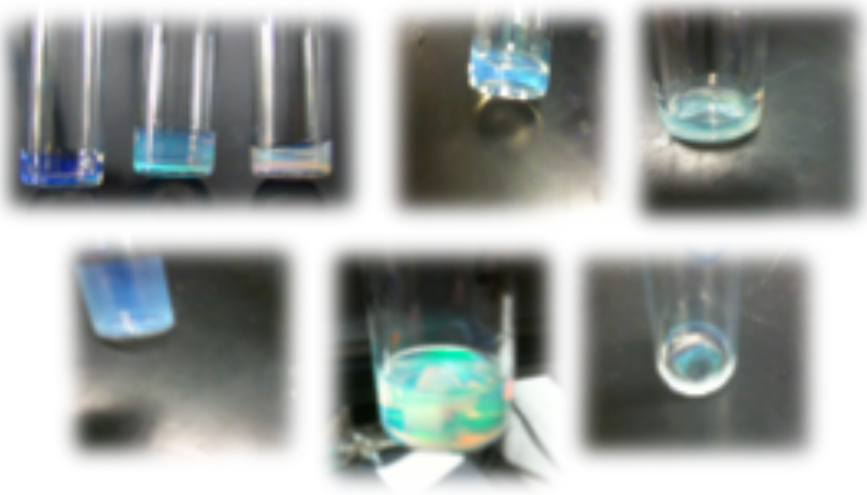

Figure 2-2. Images of the preliminary tests of self-assembled brush block copolymers from Table 2-1: Entries #1-3 are shown from left to right (top left), as well as entry #4 (top center), entry #5 (top right), entry #6 (bottom left), entry #7 (bottom center), and entry #8 (bottom right).

The racemic PLA and PS based MMs employed in this study were synthesized from *exo*-norbornene functionalized initiators, suited for the ring opening polymerization of lactide and the controlled radical polymerization of styrene. The MMs were synthesized with similar molecular weights (MWs) and narrow polydispersity indices (PDIs) (PLA: $M_n = 6.1 \times 10^3$ g/mol, PDI = 1.20; PS: $M_n = 5.7 \times 10^3$ g/mol, PDI = 1.02). More importantly, the advantageous characteristics (*i.e.* livingness, stability, functional group, and steric tolerance) of Ru-mediated ROMP enabled the sequential polymerization of the MMs to brush BCPs in high yields with controlled MWs and narrow MWDs (**Figure 2-3**). The MW of the brush BCPs were controlled by the MM to Ru ratio, and ranged from 1.08×10^6 to 6.64×10^6 g/mol, while maintaining relatively narrow MWDs (PDI = 1.07-1.58) considering the ultra-high MWs, highlighting the robustness of ROMP. For this study, we targeted blocks with near equal weight ratios with the goal of achieving lamellar nanostructures (**Table 2-2**).

Table 2-2. Molecular weight information about the (polynorbornene-*g*-polystyrene)-*b*-(polynorbornene-*g*-polylactide) polymer series. a) The molar ratios used in the synthesis of these brush block copolymers of the catalyst (C) and the MMs. b) Molecular weight and polydispersity indices as measured by GPC. c) Approximation of the size of each block as calculated using NMR and GPC results (discussed later).

Sample	C:PLA:PS [a]	$M_{n,theo}$ ($\times 10^6$ g/mol)	M_n ($\times 10^6$ g/mol)[b]	PDI (M_w/M_n)[b]	DP PLA [c]	DP PS [c]
A	1:74:78	0.90	1.08	1.07	84	98
B	1:99:105	1.20	1.53	1.09	116	142
C	1:126:132	1.52	1.99	1.12	153	182
D	1:136:144	1.65	2.38	1.22	187	215
E	1:135:142	1.63	2.68	1.16	206	246
F	1:150:158	1.81	2.94	1.17	225	271
G	1:157:166	1.90	3.19	1.26	246	292
H	1:174:183	2.10	3.32	1.29	252	309
I	1:198:210	2.40	4.02	1.34	289	391
J	1:223:237	2.71	4.21	1.36	319	391
K	1:246:262	2.99	5.80	1.5	436	543
L	1:273:288	3.30	6.64	1.58	497	624

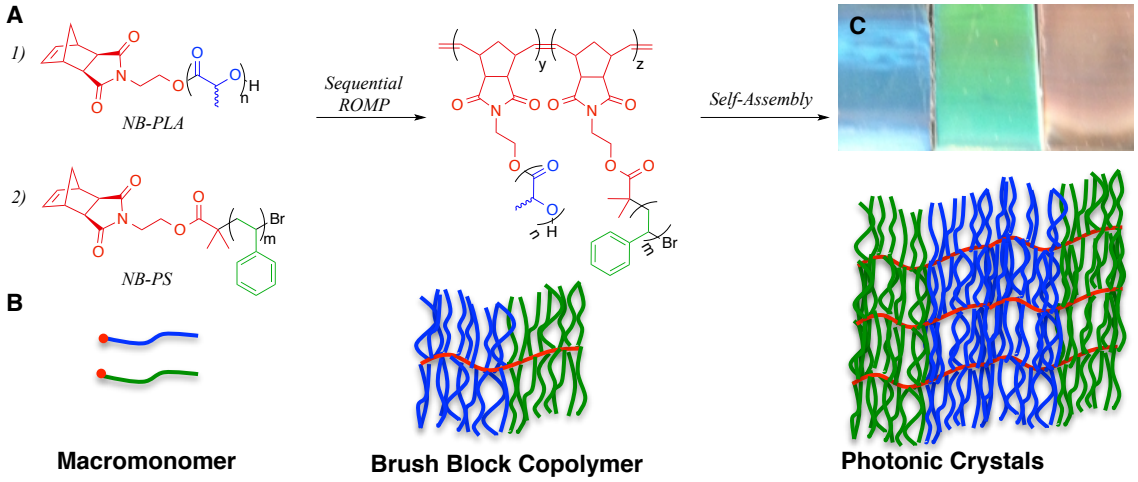

Figure 2-3. (**A**) PS and PLA based MMs were sequentially polymerized by ROMP to brush BCPs. (**B**) A schematic representation depicts the brush BCPs, and their assembly into ordered lamellar nanostructures. (**C**) Different annealing techniques render unique photonic crystals for the same brush BCP, as shown in this photograph.

After preparing a series of well-defined brush BCPs with a broad range of MWs, we investigated a number of simple self-assembly methods to yield thin, solid films. Our annealing methods included controlled evaporation from DCM and THF solutions, before and after thermal annealing, as well as direct thermal annealing of the solid polymer powder under compression between two glass substrates. The drastic effect of the assembly method on the resulting nanostructures is most starkly visualized by a single brush BCP (M_n = 2.94 × 10^6 g/mol), which appeared blue when cast from DCM, green when cast from THF, and red after thermally annealing of the green film cast from THF (**Figure 2-4**). Quantitative reflection measurements were performed on a spectrophotometer equipped with an 'integrating sphere' diffuse reflectance accessory. The reflection spectra confirm the large differences between samples prepared by different annealing procedures (**Figure 2-4A**). For the sample shown in **Figure 2-4**, the first (longest wavelength) peak of reflection shifts by hundreds of nanometers, depending on the method of film preparation. The difference in color is not due to residual solvent; the films were completely dry and we did not observe any color change upon placing a sample in high vacuum for more than 50 hours.

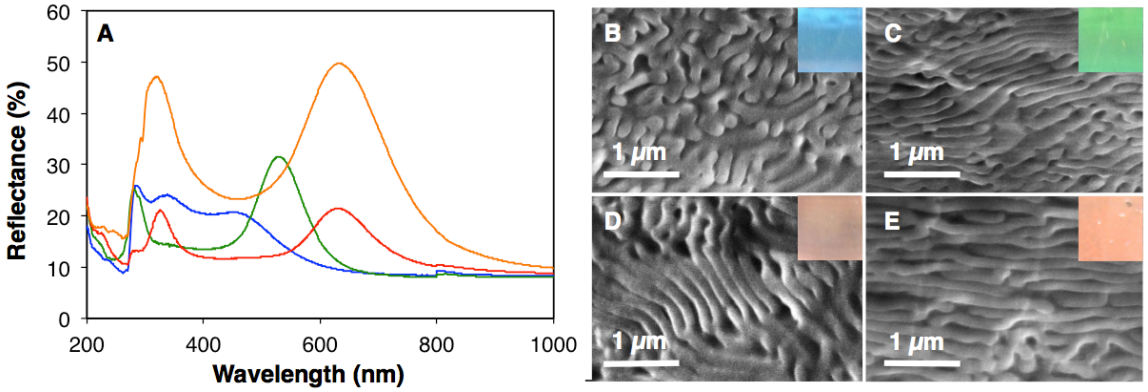

Figure 2-4. (**A**) Reflection spectra are plotted for the brush BCP (M_n = 2.94 × 10^6 g/mol) films prepared from the controlled evaporation from DCM (blue), or THF, before (green), and after (red) thermal treatment, as well as via thermal annealing under compression (orange). SEM cross-sections reveal the morphology of the middle of the brush BCP films prepared from the controlled evaporation from DCM (**B**), THF before (**C**) and after (**D**) thermal annealing, as well as by direct thermal annealing under compression (**E**). The insets show photographs of each sample.

Scanning electron micrograph (SEM) cross-sections were used to directly image the film morphologies to further investigate causes of the observed reflection spectra. Although the thermally annealed samples must be composed of larger domain sizes than the films prepared via controlled evaporation (as suggested by the greater λ_{max}), we were curious as to why the film cast from DCM provided the markedly altered reflection spectra. SEM images provided insight into the self-assembly of the films from different techniques, clearly visualizing the polymer morphologies and domain sizes (**Figure 2-4 B-E**). For this polymer, all of the films, except those prepared from DCM, showed the expected stacked lamellar morphology for symmetric BCPs. In the case of the film cast from DCM, a disordered morphology was observed in the SEM image. The evaporative self-assembly process is dictated by a number of factors, including the kinetics of evaporation, quality of solvent, PS/PLA interaction parameters, as well as the energetics of the glass/polymer interface. For many samples, the degree of lamellar order decreased as a function of distance from the glass interface. For BCPs with approximately equal volume fractions, the lamellar morphology is the most thermodynamically stable, as it minimizes the interfacial surface energy between the two constituent polymers. THF afforded larger and better ordered domains than DCM, which we attribute to the fact that it is a good solvent for this copolymer system,[31] as well as to its decreased volatility, which allows improved chain mobility to rearrange during evaporation before all the chains enter the glassy state once all solvent is removed. After thermal annealing, these samples become more ordered, with larger domain sizes, as observed in the SEMs and evidenced by the

reflection spectra. Films that were directly thermally annealed from dry polymer powder also formed well-ordered lamellae with long wavelength reflection. The improved reflection coefficient is a consequence of film thickness.

We observed the first order peak of reflection to be a linear function of MW, for all of the self-assembly techniques employed. This is in contrast to a corresponding linear copolymer system, where the domain spacing is proportional to $MW^{0.81}$.[32] Because the peak wavelength and domain spacing are directly related by the equation $\lambda_{max} = 2(n_1x_1 + n_2x_2)$,[9] our results suggest that the brush BCPs studied yield a larger increase in domain spacing per monomer incorporated than a corresponding linear system. Given the high persistence lengths of these brush polymers,[33] we rationalize this observation in terms of the degree of backbone extension enforced by the steric congestion of the brushes. Thus, the brush polymer architecture enables both a large equilibrium scaling for self-assembled structures as well as a very fast equilibration rate, due to the significantly reduced chain entanglement (even at ultra high MW).

Direct thermal annealing of the polymer powders under compression proved to be the most successful assembly technique, in that it enabled ultra-high MW polymers to reach ordered nanostructures with photonic crystal characteristics at NIR wavelengths (**Figure 2-5 E-F**). By contrast, in the case of controlled evaporation, most of the high molecular weight polymers ($M_n > 3 \times 10^6$ g/mol) did not assemble into films with distinct Bragg reflection peaks. The unmatched structural order achieved through thermal annealing is highlighted by the fact that the ultra-high MW polymers possessed photonic bandgaps well into the NIR (up to λ_{max} = 1311 nm), an unprecedented wavelength regime for unswelled BCP photonic crystals. Furthermore, the low energetic barriers to reorganization enable the application of any BCP self-assembly technique to our system to achieve improved lamellar order and optical performance. As NIR dielectric mirrors, these robust solid-state photonic crystals enable a host of exciting applications for BCPs to telecommunications and thermal radiation management.

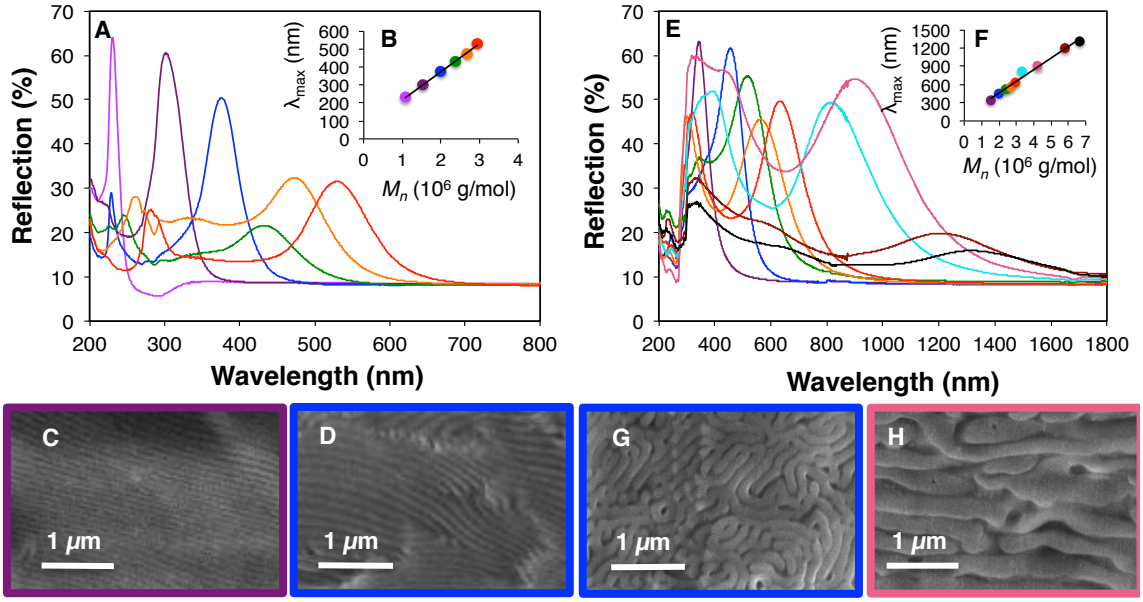

Figure 2-5. (**A**) Reflectance is plotted as a function of wavelength for the films prepared from the controlled evaporation from THF for several different MW polymers. (**B**) λ_{max} is plotted against MW for films prepared from the controlled evaporation of THF. SEM cross-sections are shown for the middle of BCP films with $M_n = 1.53 \times 10^6$ g/mol. Linear fit $R^2 = 0.997$. (**C**) and $M_n = 1.99 \times 10^6$ g/mol (**D**) prepared from the controlled evaporation of THF. (**E**) Reflectance is plotted as a function of wavelength for the films prepared by thermal annealing under compression for several different MW polymers. (**F**) λ_{max} is plotted against MW for films prepared by thermal annealing under compression. SEM cross-sections are shown for the middle of BCP films with $M_n = 1.99 \times 10^6$ g/mol. Linear fit $R^2 = 0.984$. (**G**) and $M_n = 4.21 \times 10^6$ g/mol (**H**) prepared by thermal annealing under compression.

To justify the proposed mechanism of the observed reflection spectra, transfer matrix simulations have been employed to model the reflection spectra of the polymer photonic crystals. Additionally, angle dependent reflection spectra of a well-ordered sample were measured and compared with one-dimensional transfer matrix simulations. Comparison of the experimental data with the simulations showed good agreement and strongly suggested that the observed lamellar nanostructures consist of alternating polymer layers, which represent pseudo-1D photonic crystals.[34]

CONCLUSION

In conclusion, the rapid self-assembly of high-molecular weight brush polymers was shown to work as a facile method for generating ordered nanostructures with large domain sizes, specifically pseudo-1D photonic crystals. The reduced chain entanglement of brush BCPs enables assembly of large nanostructures that reflect long wavelength light without the use of any additives. The linear trend of λ_{max} as a function of MW enables one to synthetically "dial-in" dielectric mirrors with first

order peaks spanning from the UV to NIR. We envision that materials produced through this approach have potential as NIR-reflecting building materials, for use in inhibiting the thermalization of NIR radiation in urban environments. Moreover, the functional flexibility of our approach enables a host of new directions for functional, compliant, and stimuli-responsive photonic elements.

SUPPORTING INFORMATION

Materials

$(H_2IMes)(pyr)_2(Cl)_2RuCHPh$[35] and *N*-(hydroxyethanyl)-*cis*-5-norbornene-*exo*-2,3-di-carboximide[36] were prepared as described previously. All solvents were purchased from VWR or Sigma-Aldrich. Ruthenium tetroxide was purchased form Acros Organics. Ruthenium-based metathesis catalyst was obtained from Materia Inc. and stored in a drybox. Other chemicals were bought from Sigma-Aldrich. Dry solvents were purified by passing them through solvent purification columns. 3,6-dimethyl-1,4-dioxane-2,5-dione was purified by sublimation under vacuum. All other solvents and chemicals were used without further purification unless otherwise stated.

General information

NMR spectra were recorded at room temperature on a Varian Inova 500 (at 500 MHz). The NMR spectra were analyzed on MestReNova software and are reported relative to $CDCl_3$ (δ 7.26). NMR abbreviations: s = singlet, d = doublet, t = triplet, m = multiplet, br = broad, dt = doublet of triblets.

Gel permeation chromatography (GPC) was carried out in THF on two Plgel 10 μm mixed-B LS columns (Polymer Laboratories) connected in series with a miniDAWN TREOS multiangle laser light scattering (MALLS) detector, a ViscoStar viscometer, and Optilab rex differential refractometer (all from Wyatt Technology. The d*n*/dc values used for the polylactide and polystyrene macromonomers were 0.050 and 0.180, respectively. d*n*/dc values for the brush BCPs were obtained for each injection by assuming 100% mass elution from the columns.

High resolution mass spectra (HRMS) were provided by the California Institute of Technology Mass Spectrometry Facility.

SEM images were taken on a ZEISS 1550 VP Field Emission SEM.

Reflection measurements were performed on a Cary 5000 UV/Vis/NIR spectrophotometer equipped with an 'integrating sphere' diffuse reflectance accessory (Internal DRA 1800). All measurements were referenced to a LabSphere Spectralon 99% certified reflectance standard. The samples were illuminated through a Spectralon-coated aperature with a diameter of 1 cm and a beam area of

approximately 0.5 cm^2. The samples were scanned at a rate of 600 nm/min, with a 1 nm data interval, from 1800 to 200 nm, and a detector crossover (InGaAs to PMT) at 800 nm.

Synthesis

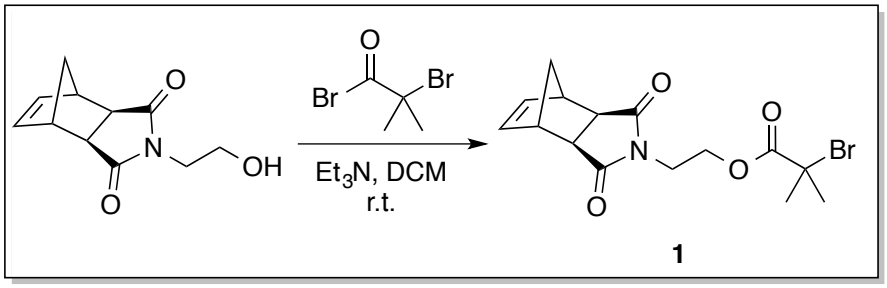

N-(2-bromo-2-methylpropanoylethanyl)-cis-5-norbornene-exo-2,3-dicarboximide (**1**)

A round bottom flask fitted with an addition funnel was flame-dried and subsequently charged with *N*-(hydroxyethanyl)-*cis*-5-norbornene-*exo*-2,3-di-carboximide (2.51 g, 12.1 mmol) and triethylamine (2.3 mL, 16 mmol). Dry dichloromethane (80 mL) was added to the addition funnel and approximately half of it was added to the reaction mixture. To the addition funnel was added 2-bromoisobutyrylbromide (2.2 mL 18 mmol). The reaction flask was submerged in an ice-water bath and the mixture in the addition funnel added drop wise to the reaction flask. When the addition was completed the reaction mixture was allowed to stir at room temperature for 20 hours. The reaction mixture was washed with 0.1 N HCl (25 mL), $NaHCO_3$ (25 mL), and brine (2 × 25 mL), and then dried over $MgSO_4$ and concentrated in vacuo. The product was purified by silica gel chromatography (dichloromethane) to give the product, **1**, as a white solid in 66 % yield (2.87 g, 8.0 mmol). ^{1}H NMR (500 MHz, $CDCl_3$): δ (ppm) 6.28 (t, J = 1.8 Hz, 2H), 4.34-4.32 (m, 2H), 3.82-3.80 (m, 2H), 3.28-3.26 (m, 2H), 2.70 (d, J = 1.4 Hz, 2H), 1.89 (s, 6H), 1.54-1.50 (m, 1H), 1.31 (d, J = 9.9 Hz, 1H). ^{13}C NMR (500 MHz, $CDCl_3$): δ (ppm) 177.7, 171.3, 137.8, 62.6, 55.4, 47.8, 45.2, 42.9, 37.3, 30.6. HRMS (EI+): calcd. for $C_{15}H_{18}O_4NBr$ $[M+H]^+$: *m/z* = 355.0419; found 355.0435. IR (Thin Film, NaCl): 3456, 3065, 2981, 2881, 1774, 1739, 1703, 1464, 1450, 1426, 1392, 1371, 1360, 1328, 1283, 1215, 1192, 1159, 1110, 1037, 1014, 990, 942, 902, 883, 854, 828, 813, 804, 781, 771, 722 cm^{-1}.

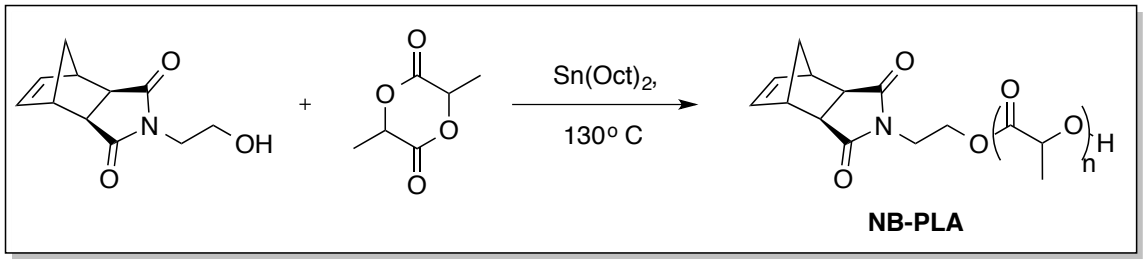

Synthesis of Norbornene-Polylactide (**NB-PLA**)

A flame-dried Schlenck tube was charged with *N*-(hydroxyethanyl)-*cis*-5-norbornene-*exo*-2,3-dicarboximide (233.9 mg, 1.13 mmol) and 3,6-dimethyl-1,4-dioxane-2,5-dione (6.096g, 42.3 mmol) along with tin-(II)-2-ethylhexanoate (≈2 mg, ≈5 μmol). This mixture was put under three vacuum-argon cycles and then allowed to stir at 130° C for 2.5 hours. After cooling to room temperature the product was dissolved in dichloromethane, filtered through a small pad of celite to remove catalyst, and precipitated into cold MeOH. ^{1}H NMR (500 MHz, $CDCl_3$): δ (ppm) 6.28 (br t, 2H), 5.25-5.03 (m, 82 H), 4.40-4.21 (m , 3H), 3.82-3.68 (m, 2H) 3.26 (s, 2H), 2.70 (m, 2H), 1.73-1.39 (m, 247H), 1.23 (br d, J = 8.5 Hz, 1H). M_n = 6.1 kg/mol. GPC-MALLS: M_n = 6.3 kg/mol, M_w/M_n = 1.20.

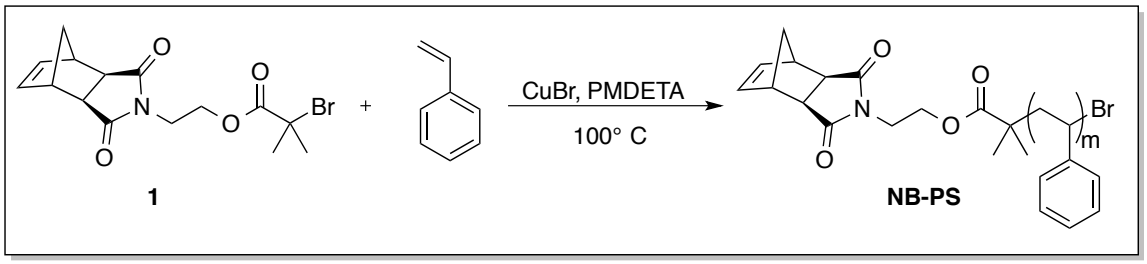

Synthesis of Norbornene-Polystyrene (**NB-PS**)

Styrene (24 mL, 0.209 mol) was passed through basic aluminum oxide and added to an oven-dried Schlenk tube fitted with a septum. Then the styrene underwent three freeze-pump-thaw cycles and was subsequently frozen again. CuBr (77.0 mg, 0.54 mmol) was next added to the frozen styrene under argon. This mixture was put under three vacuum-argon cycles before allowing the styrene to melt under argon. PMDETA (108 μL, 0.52 mmol) was then added to the mixture via a microsyringe and the solution stirred for 5 minutes. The initiator, **1** (670.4 mg, 1.88 mmol), was subsequently added to the Schlenck tube via syringe and the reaction mixture stirred at 100° C. The reaction was

stopped after 4 hours, by cooling it quickly down to room temperature using dry ice and adding THF to the mixture. The product was passed through neutral aluminum oxide to remove catalyst and precipitated into MeOH. The product was purified by repeated precipitations into MeOH until no remaining styrene was observed by NMR and further purified by silica gel chromatography (dichloromethane). ^{1}H NMR (500 MHz, $CDCl_3$): δ (ppm) 7.25-6.29 (br m, 260 H), 6.28 (br s, 2H), 4.59-4.35 (m, 1H), 3.65-3.32 (m, 4H), 3.22 (br s, 2H), 2.62 (br d, J = 6.6 Hz, 2 H), 2.56-1.55 (br m, 105 H), 0.99-0.83 (m, 6H). M_n = 5.8 kg/mol. GPC-MALLS: M_n = 6.1 kg/mol, M_w/M_n = 1.02.

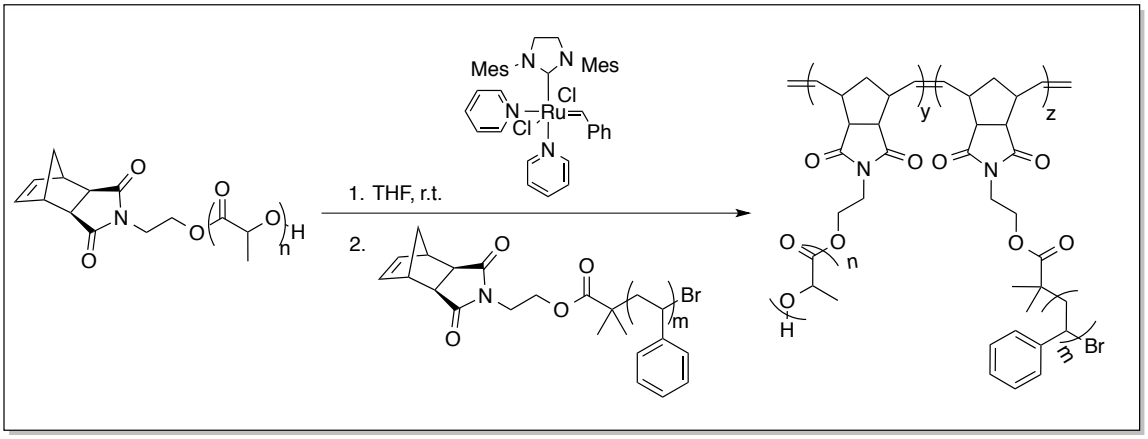

General Procedure for Block Copolymerization of Two Macromonomers via ROMP (**A-L**)

In a typical experiment, 150 mg of each of the macromonomers were added to separate vials. The desired amount of catalyst was added to the third vial. The vials were brought into a drybox and the macromonomers were dissolved in the desired amount of THF ($[M]_0 \approx 0.05$ M), while the catalyst was dissolved in 1.00 mL of THF. The desired amount of catalyst solution was injected via a microsyringe into the solution of the NB-PLA, as it polymerizes faster.[28] When the first macromonomer had polymerized, the solution of the second macromonomer (NB-PS) was added to the reaction mixture. This solution was allowed to stir for an additional 2-3 hours. The reaction was moved out of the dry box, quenched with butyl vinyl ether, and isolated by precipitation into MeOH. Conversion was 100% based on RI traces from the GPC, and isolated yields were generally over 85%.

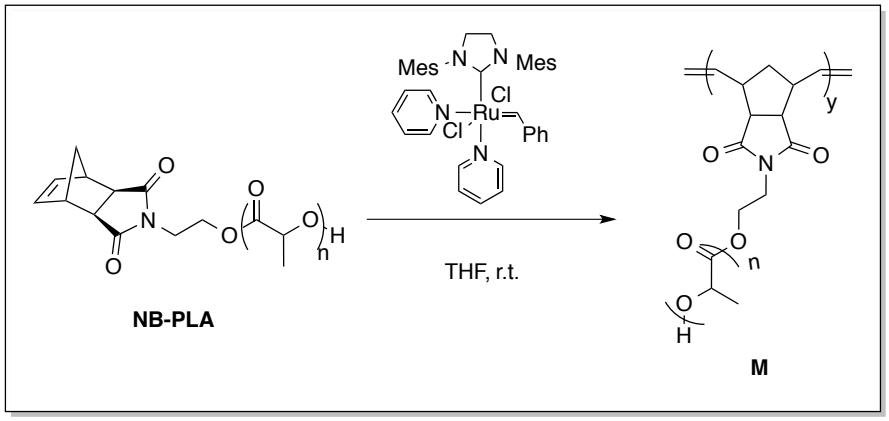

Synthesis of a Polylactide Brush Homopolymer (**M**)

NB-PLA (62.0 mg, 10.2 μmol) was weighed into a vial. The catalyst (2.6 mg, 3.58 μmol) was added to a separate vial. The vials were brought into the drybox and the NB-PLA was dissolved in THF (250 μL), while the catalyst was dissolved in 1.00 mL of THF. The catalyst solution (17 μL, 0.061 μmol) was injected via a microsyringe into the solution of macromonomers and the solution allowed to stir for 2 hours. The reaction was moved out of the dry box, quenched with butyl vinyl ether, and isolated by precipitation into MeOH. GPC-MALLS: M_n = 1.04 x 10^6 g/mol, M_w/M_n = 1.03.

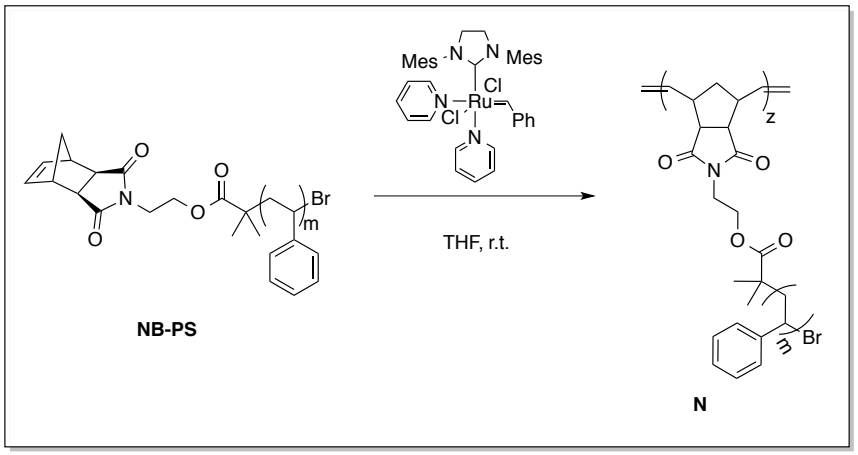

Synthesis of a Polystyrene Brush Homopolymer (**N**)

NB-PS (52.9 mg, 9.12 μmol) was weighed into a vial. The catalyst (2.6 mg, 3.58 μmol) was added to a separate vial. The vials were brought into the drybox and the NB-PS was dissolved in THF

(200 μL), while the catalyst was dissolved in 1.00 mL of THF. The catalyst solution (14.5 μL, 0.052 μmol) was injected via a microsyringe to the solution of macromonomers and the solution allowed to stir for 2 hours. The reaction was moved out of the dry box, quenched with butyl vinyl ether, and isolated by precipitation into MeOH. GPC-MALLS: M_n = 1.14 x 10^6 g/mol, M_w/M_n = 1.04.

Annealing by Slow Evaporation

The solid polymer (≈40-50 mg) was put in a vial and dissolved there in approx. 10 mL of solvent (DCM or THF). Then a glass substrate was put vertically into the vial and the solvent allowed to evaporate at room temperature. The glass substrate could be subsequently annealed at 120°C in an oven for 2 hours.

Thermal annealing between two glass substrates

The solid polymer (≈ 10 mg) was sandwiched between two glass substrates and compressed with a clamp. The glass substrates, now clamped together, are then heated in an oven or a vacuum chamber at 140° C for 30 minutes.

SEM sample preparation

The samples were fractured on glass substrates and exposed to fresh RuO_4 vapor for ≈ 8 minutes.

Calculations

The degree of polymerization (DP) of each MM in the final brush BCPs, shown in **Table 2-2**, was estimated using NMR data. The total molecular weight, measured by GPC-MALLS, was the sum of the molecular weight of each brush times the DP of that brush (**eq. 1**).

$$M_{n,tot} = DP_{PLA} \times M_{n,PLA} + DP_{PS} \times M_{n,PS} \quad \textbf{(1)}$$

The M_n of the PS had been calculated by using the integration value, herein assigned *a*, of the peak at δ 6.29 -7.25ppm to the norbornene olefin peak at δ 6.28 ppm. Likewise, the M_n of the PLA had been calculated by using the integration value, herein assigned *b*, of the peak at δ 5.03-5.25 ppm to the norbornene olefin peak at δ 6.28 ppm. The two MMs did not have any overlapping peaks in that area, so they could be used as identifying peaks in the brush BCPs where the integration value of the PS peak was assigned as *x* and the integration value of the PLA peak was assigned as *y*. The ratio of *x* over *y* remained the same as the ratio of *a* multiplied by the DP of the PS block over *b* multiplied by the DP of the PLA block, as shown in **eq. 2**.

$$\frac{x}{y} = \frac{a \times DP_{PS}}{b \times DP_{PLA}} \quad \textbf{(2)}$$

If we isolate DP_{PS}/DP_{PLA} and assign it the value *c,* we obtain the following equation:

$$c = \frac{DP_{PS}}{DP_{PLA}} = \frac{\frac{x}{y}}{\frac{a}{b}} \quad \textbf{(3)}$$

Then we can add DP_{PLA}/DP_{PLA} to both sides of the equation and obtain:

$$\frac{DP_{PLA} + DP_{PS}}{DP_{PLA}} = 1 + c \quad \textbf{(4)}$$

which can be rearranged to:

$$mol\%\ (PLA) = \frac{DP_{PLA}}{DP_{PLA} + DP_{PS}} = \frac{1}{1+c} \quad \textbf{(5)}$$

to find the mol % of the PLA in the brush block copolymer. The mol % of the PS then becomes:

$$mol\%\ (PS) = \frac{DP_{PS}}{DP_{PLA}+DP_{PS}} = \frac{c}{1+c} \quad \textbf{(6)}$$

With the mol % it becomes simple to calculate the wt % of each MM by multiplying the mol percentages by the molecular weights of their respective MMs:

$$wt\%\ (PS) = \frac{mol\%(PS)\times M_{n,PS}}{mol\%(PS)\times M_{n,PS}+mol\%(PLA)\times M_{n,PLA}} \quad \textbf{(7)}$$

and the DPs can be found by multiplying the weight percentages by the total molecular weight of the brush block copolymer and dividing by molecular weight of the MMs.

$$DP_{PS} = \frac{wt\%(PS)\times M_{n,tot}}{M_{n,PS}} \quad \textbf{(8)}$$

Supplementary Figures

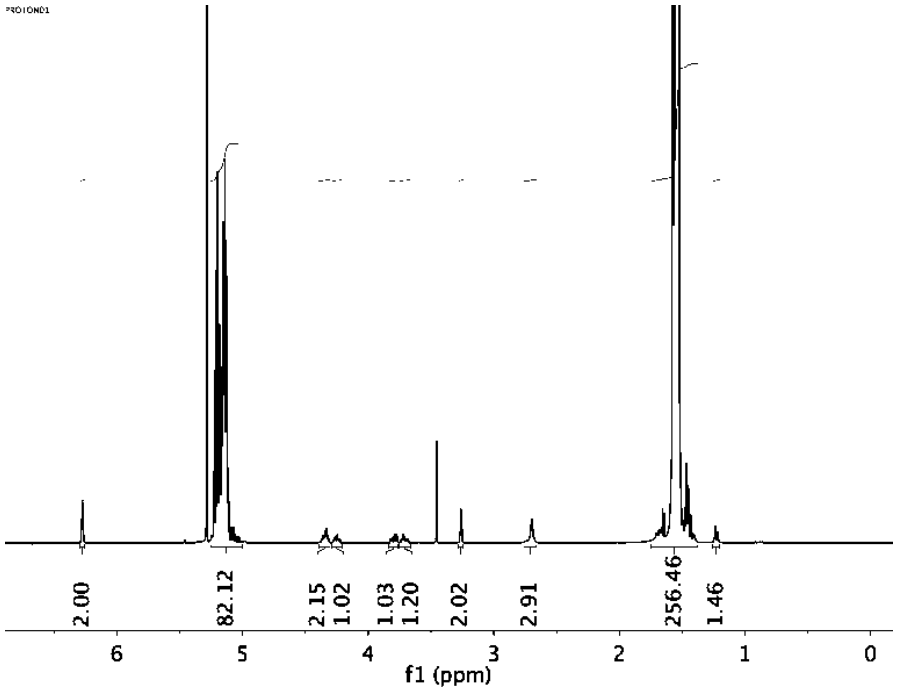

Figure 2-6. ^{1}H NMR spectra of NB-PLA.

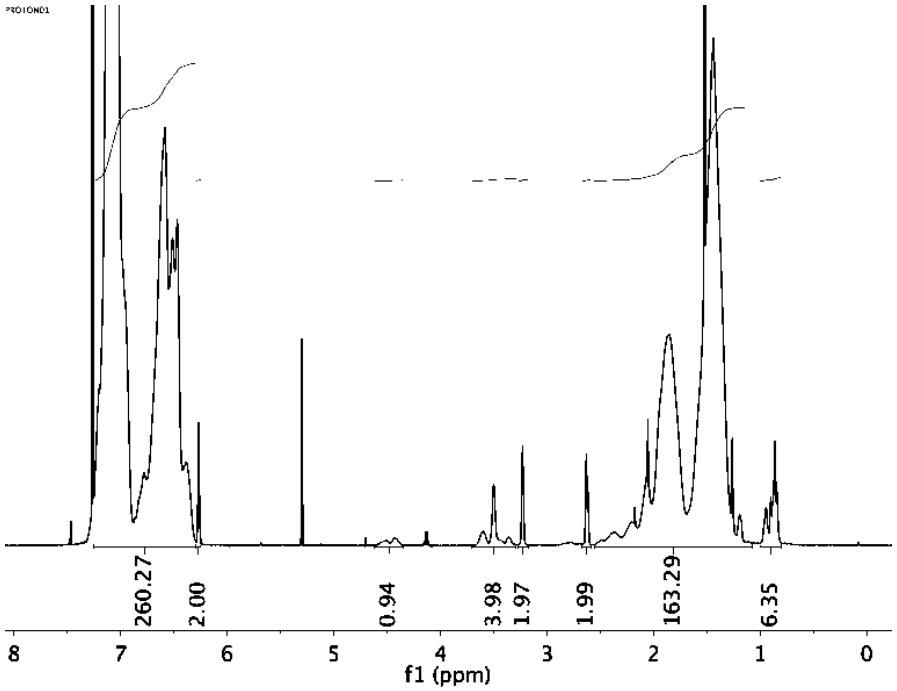

Figure 2-7. ^{1}H NMR spectra of NB-PS.

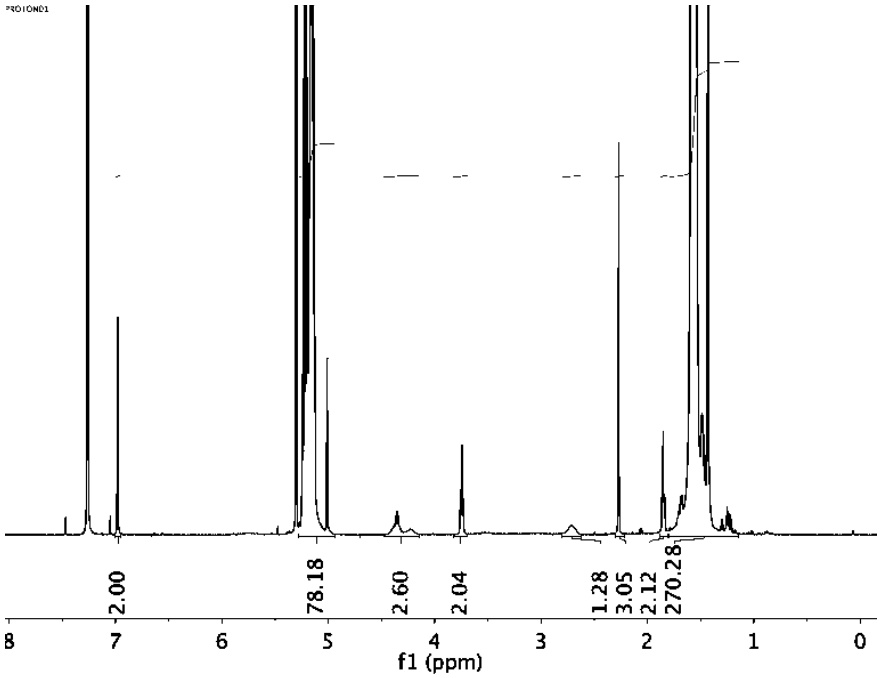

Figure 2-8. ^{1}H NMR spectra of **M** (a polylactide brush homopolymer).

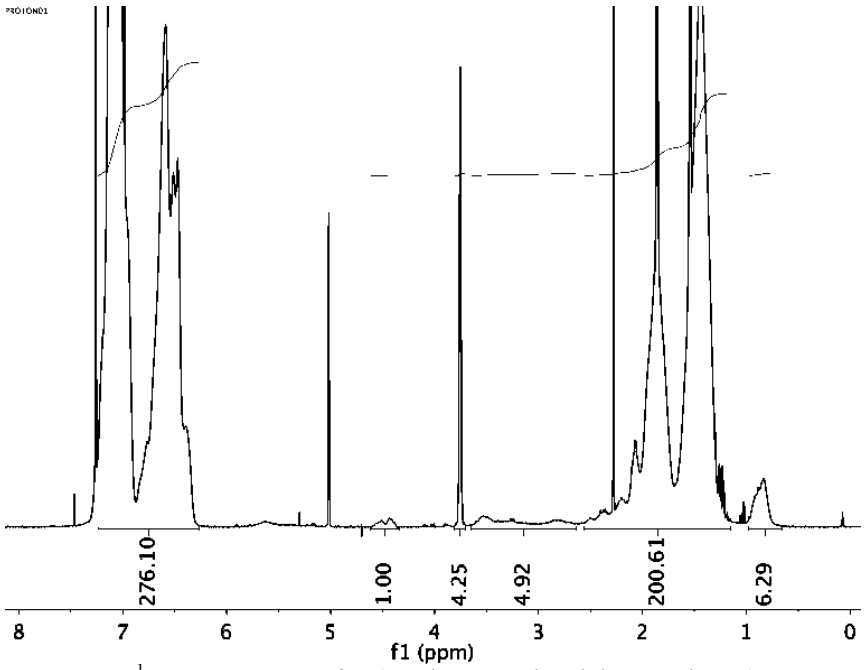

Figure 2-9. ^{1}H NMR spectra of **N** (a polystyrene brush homopolymer).

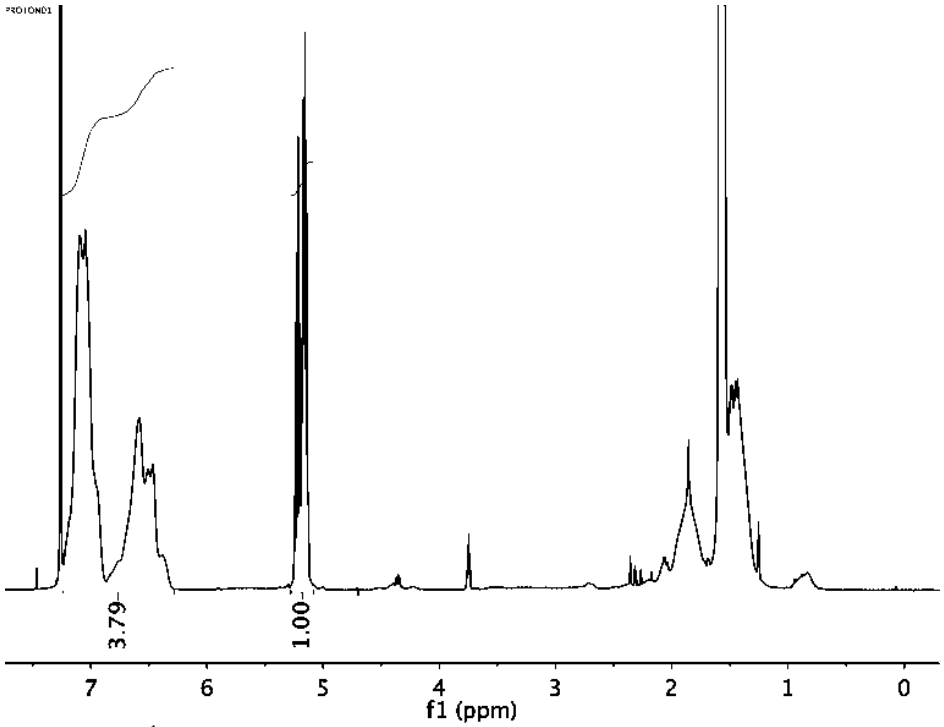

Figure 2-10. ^{1}H NMR spectra of **E** as an example of a brush block copolymer NMR spectra.

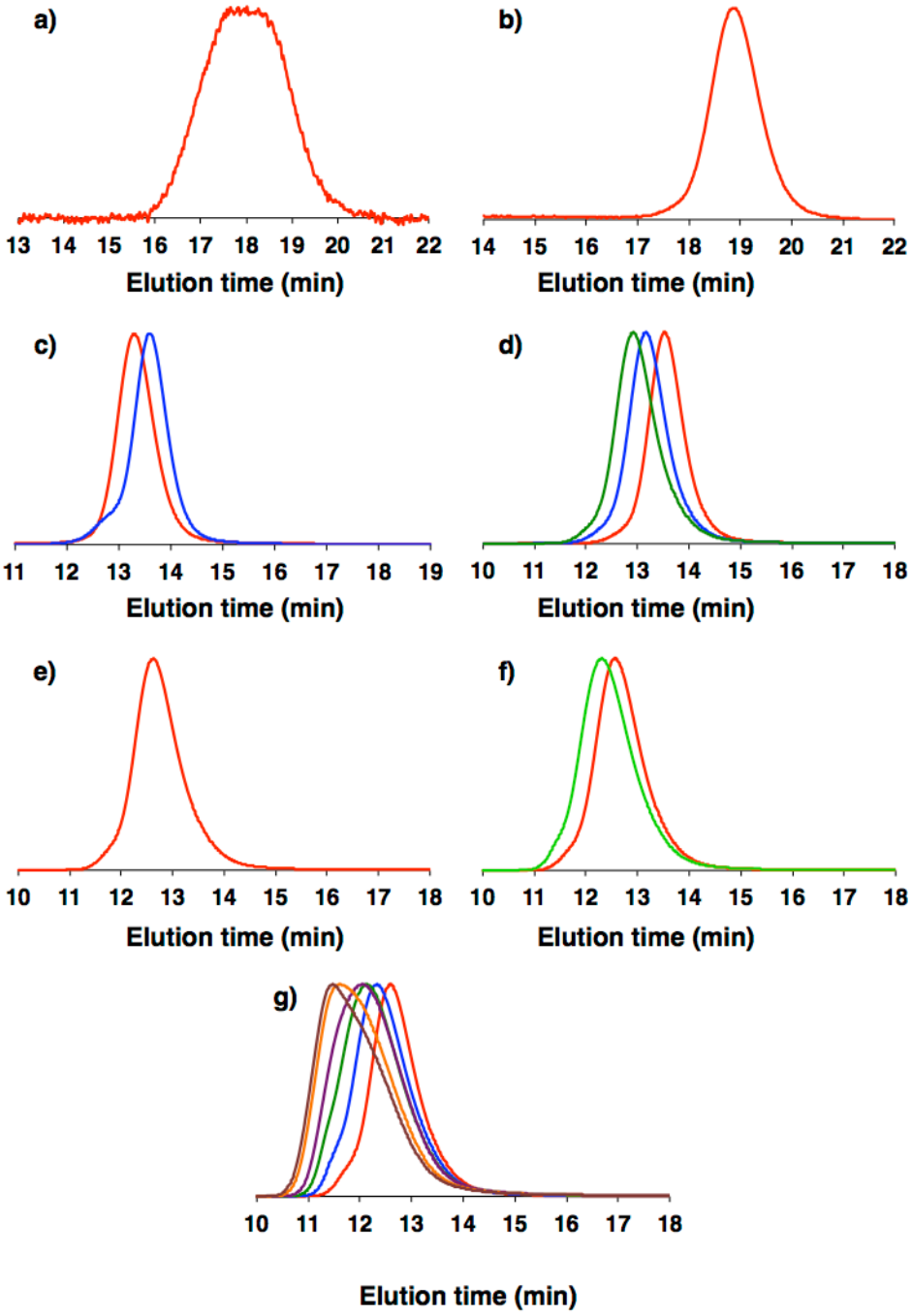

Figure 2-11. GPC RI traces of the polymers synthesized using NB-PLA, NB-PS, or both. All traces were obtained from polymers purified by precipitation into methanol. Each figure represents a single sample or a group of samples that were measured as one sample set. Traces in d-g are from samples in Table 2-2. (a) NB-PLA; (b) NB-PS; (c) red: **M**; blue: **N**; (d) red: **A**; blue: **B**; green: **C**; (e) **E**; (f) red: **D**; green: **G**; (g) red: **F**; blue: **H**; green: **I**; purple: **J**; orange: **K**; brown: **L**.

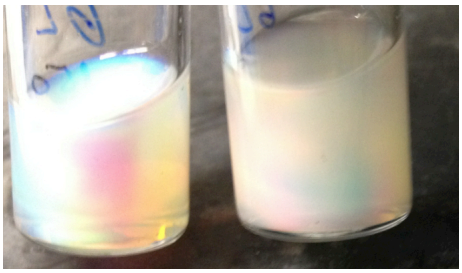

Figure 2-12. A solution of a brush block copolymer reaction solution that turned colored even while it was still in solution.

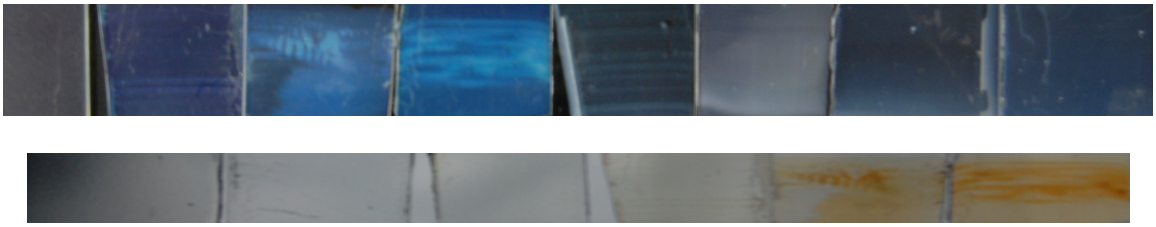

Figure 2-13. Top: Reflection of films of the brush block copolymers made by controlled evaporation from DCM. From left to right are samples **A-H** as described in Table 2-2. Bottom: Transmission of films of the brush block copolymers made by controlled evaporation from DCM. From left to right are samples **A-F** as described in Table 2-2.

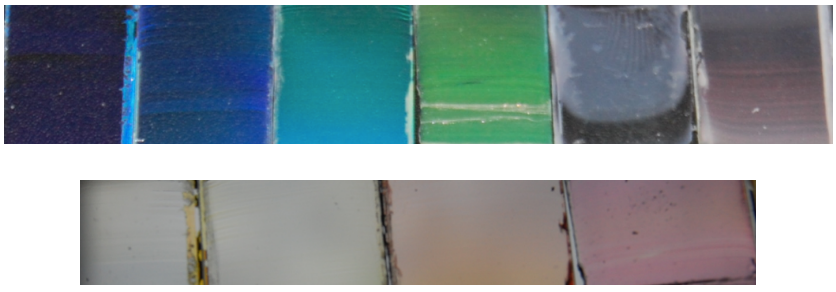

Figure 2-14. Top: Reflection of films of the brush block copolymers made by controlled evaporation from THF. From left to right are samples **C-H** as described in Table 2-2. Bottom: Transmission of films of the brush block copolymers made by controlled evaporation from THF. From left to right are samples **C-F** as described in Table 2-2.

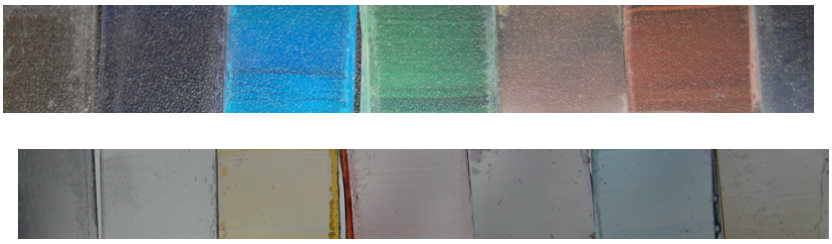

Figure 2-15. Top: Reflection of films of the brush block copolymers made by controlled evaporation from THF after heating. From left to right are samples **A-G** as described in Table 2-2. Bottom: Transmission of films of the brush block copolymers made by controlled evaporation from THF after heting. From left to right are samples **A-G** as described in Table 2-2.

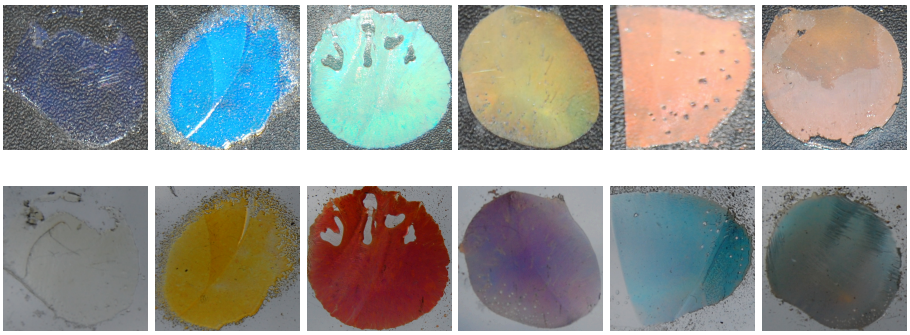

Figure 2-16. Top: Reflection of films of the brush block copolymers made by thermal compression. From left to right are samples **B-G** as described in Table 2-2. Bottom: Transmission of films of the brush block copolymers made by thermal compression. From left to right are samples **B-G** as described in Table 2-2.

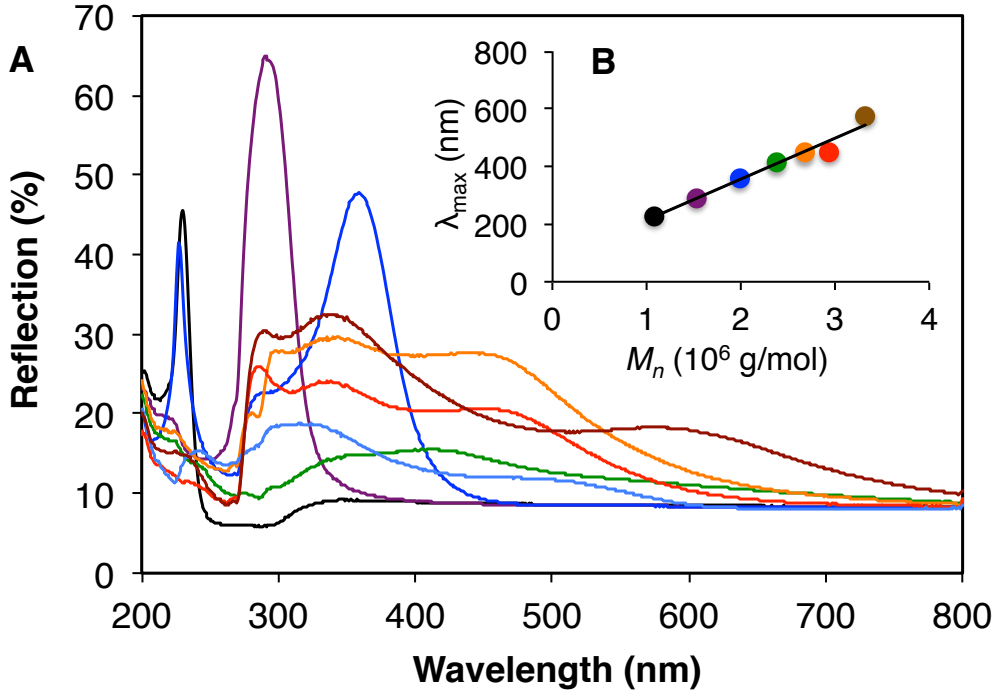

Figure 2-17. A) Plot of reflectance as a function of wavelength for the films prepared from the controlled evaporation from DCM. B) Plot of λ_{max} versus BCP MW for films prepared from the controlled evaporation from DCM.

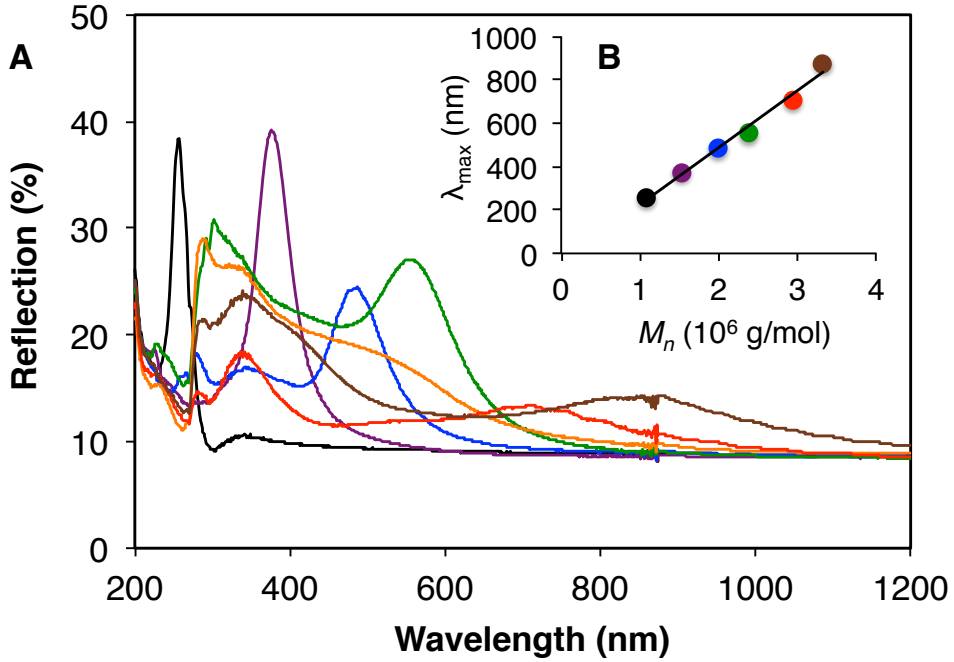

Figure 2-18. A) Plot of reflectance as a function of wavelength for the films prepared from the controlled evaporation from DCM after heating. B) Plot of λ_{max} versus BCP MW for films prepared from the controlled evaporation from DCM after heating.

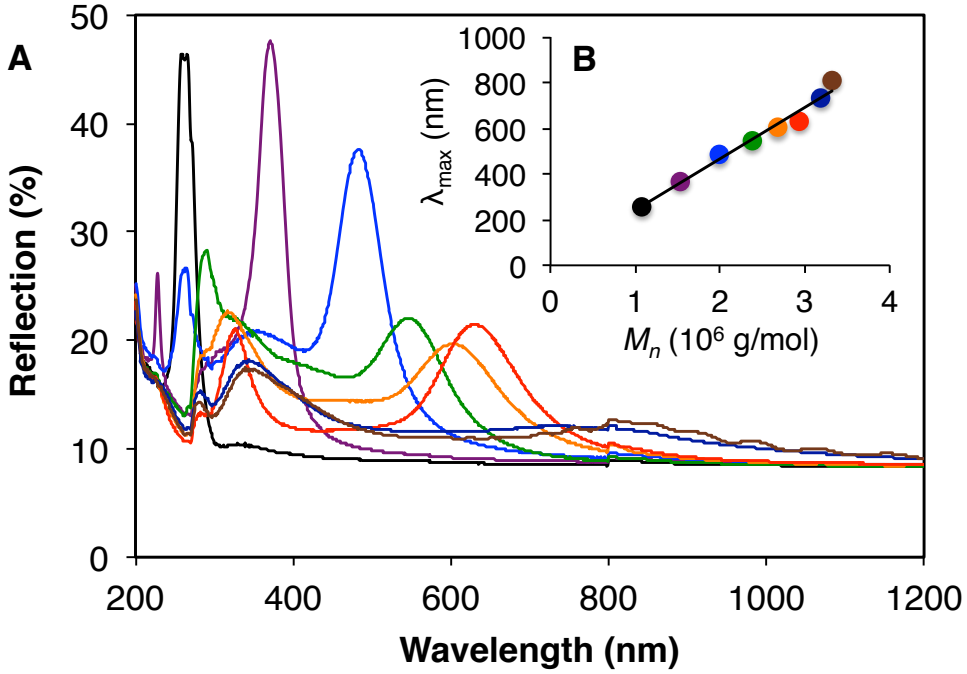

Figure 2-19. A) Plot of reflectance as a function of wavelength for the films prepared from the controlled evaporation from THF after heating. B) Plot of λ_{max} versus BCP MW for films prepared from the controlled evaporation from THF after heating.

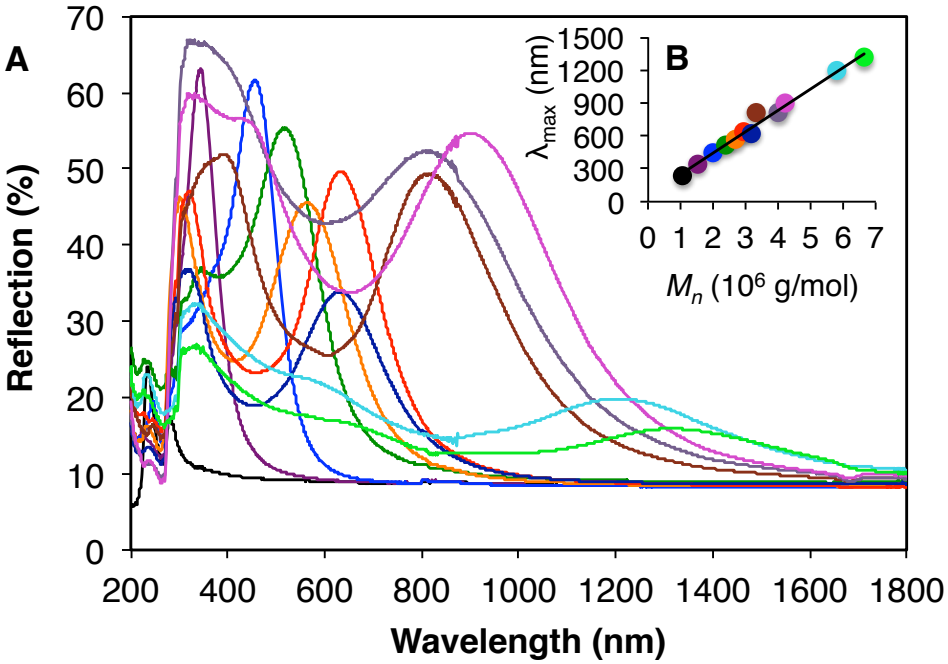

Figure 2-20. A) Plot of the reflectance as a function of wavelength for the polymer side of films prepared from thermal compression. B) Plot of λ_{max} versus BCP MW for the polymer side of films prepared from thermal compression.

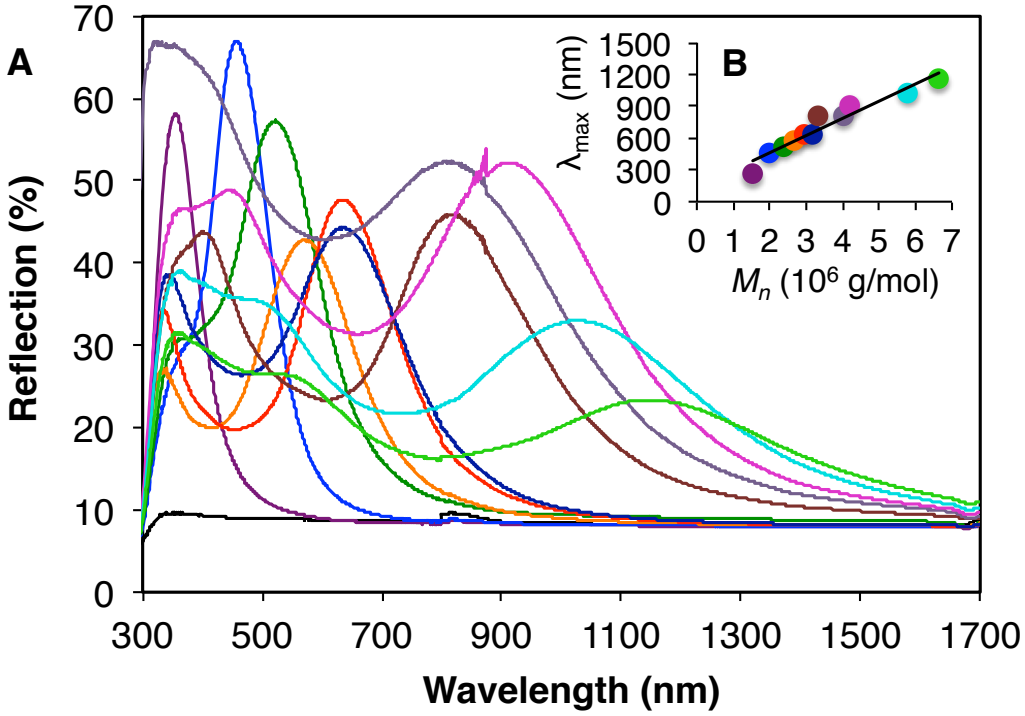

Figure 2-21. A) Plot of the reflectance as a function of wavelength for the glass side of films prepared from thermal compression. B) Plot of λ_{max} versus BCP MW for the glass side of films prepared from thermal compression.

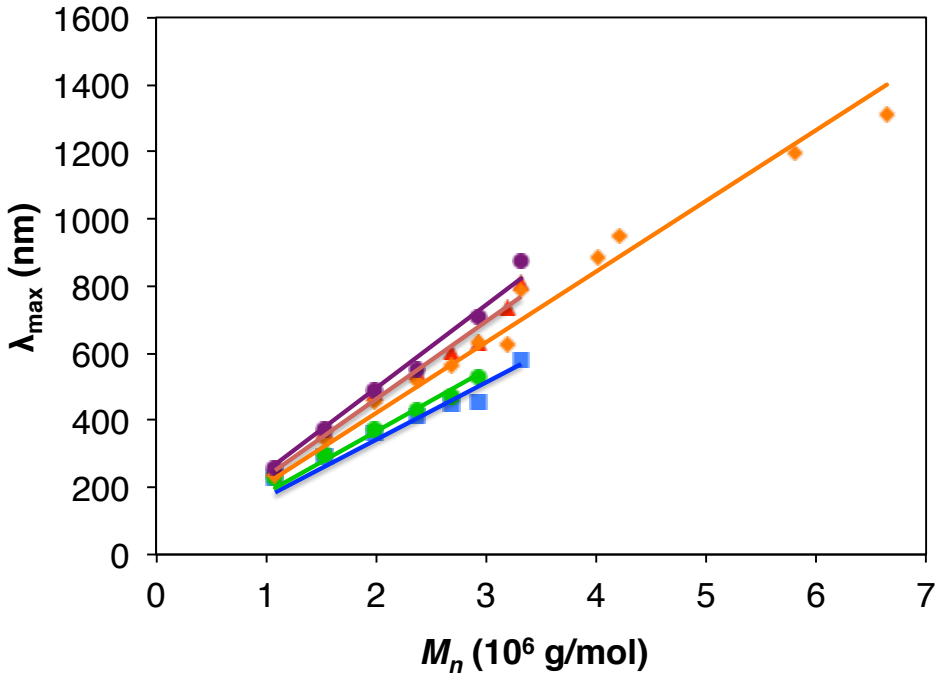

Figure 2-22. Plot of λ_{max} versus BCP MW for the glass side of films prepared from controlled evaporation out of DCM, before (blue) and after (purple) heating, or THF, before (green) and after (red) heating, as well as by thermal compression (orange).

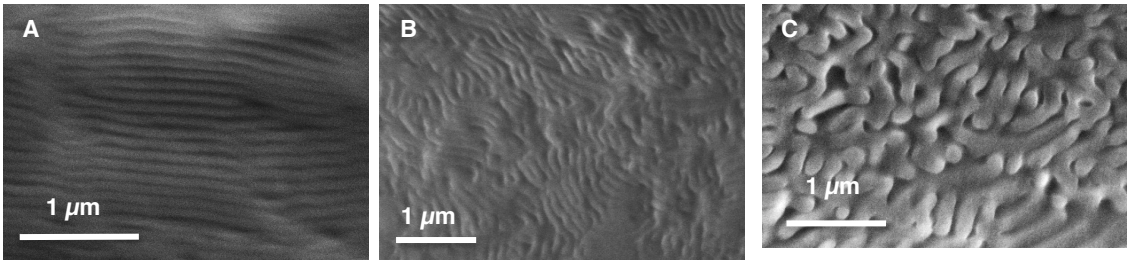

Figure 2-23. SEM image of the center of a cross-section of A) **B** (M_n = 1.53 × 10^6 g/mol) and B) **C** (M_n = 1.99 × 10^6 g/mol) and C) **F** (M_n = 2.94 × 10^6 g/mol) prepared by controlled evaporation from DCM before heating.

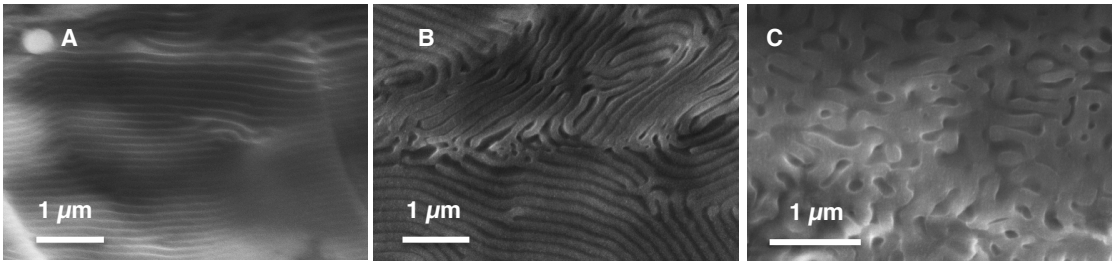

Figure 2-24. SEM image of the center of a cross-section of A) **B** (M_n = 1.53 × 10^6 g/mol) B) **C** (M_n = 1.99 × 10^6 g/mol) and C) **F** (M_n = 2.94 × 10^6 g/mol) prepared by controlled evaporation from DCM after heating.

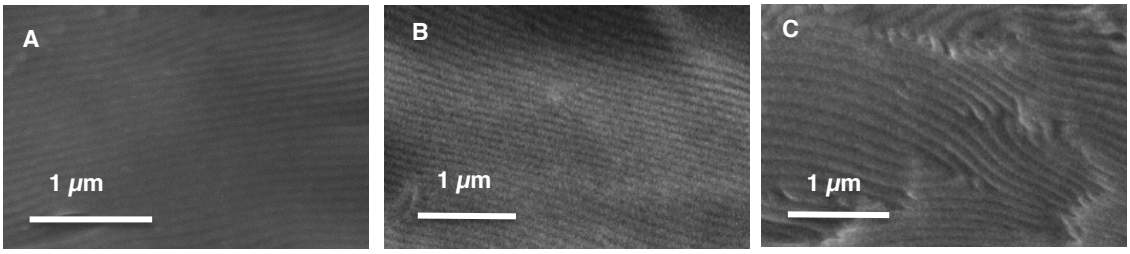

Figure 2-25. SEM image of the center of a cross-section of A) **B** (M_n = 1.53 × 10^6 g/mol) B) **C** (M_n = 1.99 × 10^6 g/mol) and C) **F** (M_n = 2.94 × 10^6 g/mol) prepared by controlled evaporation from THF before heating.

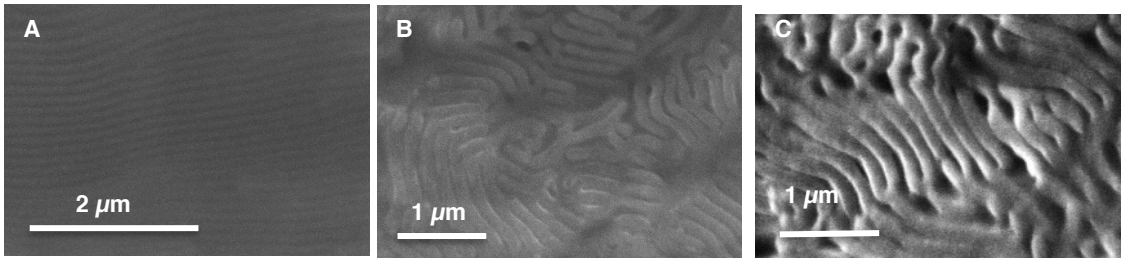

Figure 2-26. SEM image of the center of a cross-section of A) **B** (M_n = 1.53 × 10^6 g/mol) B) **C** (M_n = 1.99 × 10^6 g/mol) and C) **F** (M_n = 2.94 × 10^6 g/mol) prepared by controlled evaporation from THF after heating.

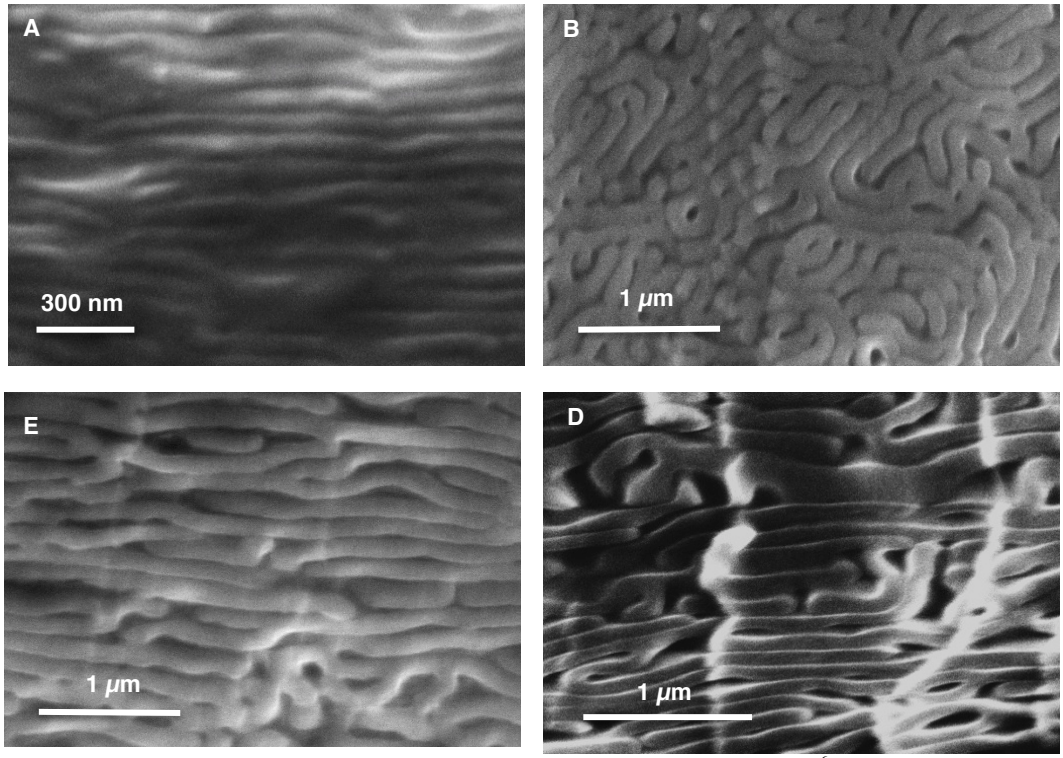

Figure 2-27. SEM image of the center of a cross-section of A) **B** (M_n = 1.53 × 10^6 g/mol) B) **C** (M_n = 1.99 × 10^6 g/mol), C) **F** (M_n = 2.94 × 10^6 g/mol) and D) **K** (M_n = 5.80 × 10^6 g/mol) prepared by controlled evaporation from THF after heating.

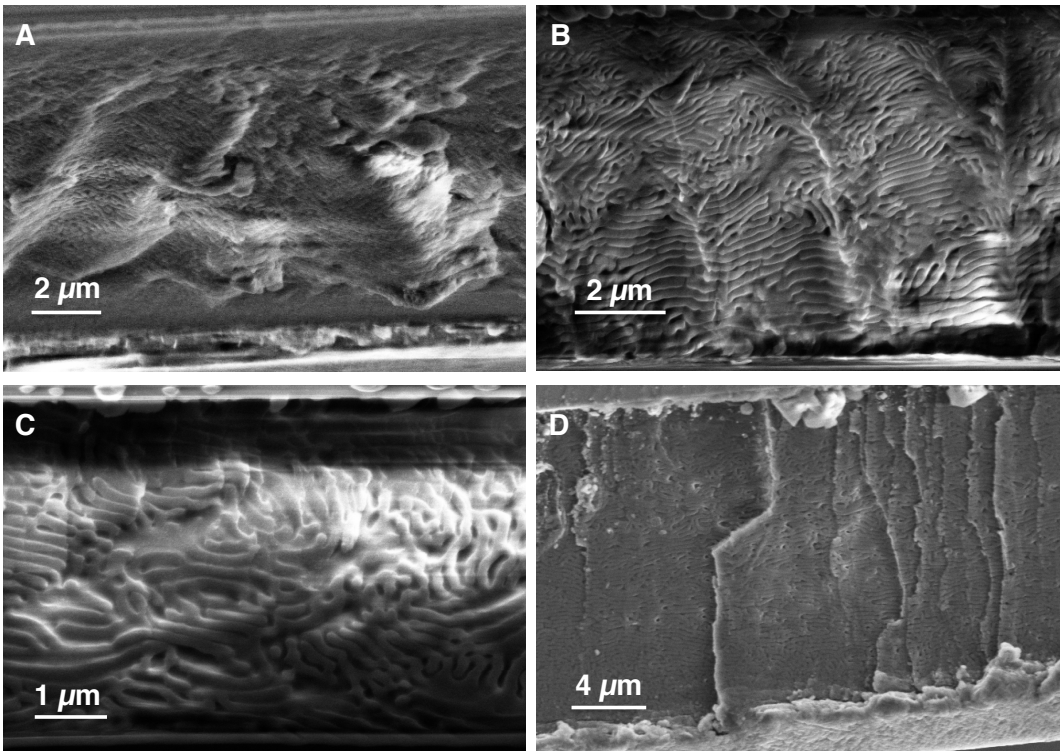

Figure 2-28. SEM image of the thickness of a cross-section of **F** (M_n = 2.94 × 10^6 g/mol) prepared by A) controlled evaporation from DCM, B) controlled evaporation from THF before heating, and C) after heating as well as D) prepared by thermal compression.

This shows that the thermally compressed film is significantly thicker than the films made from controlled evaporation. B) and C) also show that of the samples reflecting light, even the higher molecular weight films prepared by controlled evaporation from THF showed a lamellar orientation.

REFERENCES AND NOTES:

(1) Bates, F. S.; Hillmyer, M. A.; Lodge, T. P.; Bates, C. M.; Delaney, K. T.; Fredrickson, G. H. *Science.* **2012**, *336*, 434.

(2) Fasolka, M. J.; Mayes, A. M. *Annu. Rev. Mater. Res.* **2001**, *31*, 323.

(3) Thomas, E. L.; Lescanec, R. L. *Phil. Trans. R. Soc. Lond. A* **1994**, *348*, 149.

(4) Grubbs, R. B. *J. Polym. Sci. Part A Polym. Chem.* **2005**, *43*, 4323.

(5) Fink, Y.; Urbas, A. M.; Bawendi, M. G.; Joannopoulos, J. D.; Thomas, E. L. *J. Light. Technol.* **1999**, *17*, 1963.

(6) Ge, J.; Yin, Y. *Angew. Chem. Int. Ed.* **2011**, *50*, 1492.

(7) Joannopoulos, J. D. *Photonic Crystals: Molding The Flow of Light*; Princeton University Press, 2008.

(8) Kang, Y.; Walish, J. J.; Gorishnyy, T.; Thomas, E. L. *Nat. Mater.* **2007**, *6*, 957.

(9) Edrington, A. C.; Urbas, A. M.; DeRege, P.; Chen, C. X.; Swager, T. M.; Hadjichristidis, N.; Xenidou, M.; Fetters, L. J.; Joannopoulos, J. D.; Fink, Y.; Thomas, E. L. *Adv. Mater.* **2001**, *13*, 421.

(10) Chow, T.; Li, C.; Lin, Z. *Sol. Energy Mater. Sol. Cells* **2010**, *94*, 212.

(11) Urbas, A.; Fink, Y.; Thomas, E. L. *Macromolecules* **1999**, *32*, 4748.

(12) Urbas, A.; Sharp, R.; Fink, Y.; Thomas, E. L.; Xenidou, M.; Fetters, L. J. *Adv. Mater.* **2000**, *12*, 812.

(13) Parnell, A. J.; Pryke, A.; Mykhaylyk, O. O.; Howse, J. R.; Adawi, A. M.; Terrill, N. J.; Fairclough, J. P. A. *Soft Matter* **2011**, *7*, 3721.

(14) Lee, I.; Kim, D.; Kal, J.; Baek, H.; Kwak, D.; Go, D.; Kim, E.; Kang, C.; Chung, J.; Jang, Y.; Ji, S.; Joo, J.; Kang, Y. *Adv. Mater.* **2010**, *22*, 4973.

(15) Noda, S.; Tomoda, K.; Yamamoto, N.; Chutinan, A. *Science* **2000**, *289*, 604.

(16) Lin, S. Y.; Fleming, J. G.; Hetherington, D. L.; Smith, B. K.; Zubrzycki, W.; Kurtz, S. R.; Bur, J. *Nature* **1998**, *394*, 251.

(17) Masuda, H.; Ohya, M.; Asoh, H.; Nakao, M.; Nohtomi, M.; Tamamura, T. *Jpn. J. Appl. Phys.* **1999**, *38*, L1403.

(18) Birner, A.; Wehrspohn, R. B.; Gösele, U. M.; Busch, K. *Adv. Mater.* **2001**, *13*, 377.

(19) Wanke, M. C.; Lehman, O.; Müller, K.; Wen, Q.; Stuke, M. *Science* **1997**, *275*, 1284.

(20) Shoji, S.; Kawata, S. *Appl. Phys. Lett.* **2000**, *76*, 2668.

(21) Campbell, M.; Sharp, D. N.; Harrison, M. T.; Denning, R. G.; Turberfield, A. J. *Nature* **2000**, *404*, 53.

(22) Braun, P. V; Wiltzius, P. *Nature* **1999**, *402*, 603.

(23) Bertone, J. F.; Jiang, P.; Hwang, K. S.; Mittleman, D. M.; Colvin, V. L. *Phys. Rev. Lett.* **1999**, *83*, 300.

(24) Runge, M. B.; Dutta, S.; Bowden, N. B. *Macromolecules* **2006**, *39*, 498.

(25) Runge, M. B.; Bowden, N. B. *J. Am. Chem. Soc* **2007**, *129*, 10551.

(26) Runge, M. B.; Lipscomb, C. E.; Ditzler, L. R.; Mahanthappa, M. K.; Tivanski, A. V.; Bowden, N. B. *Macromolecules* **2008**, *41*, 7687.

(27) Rzayev, J. *Macromolecules* **2009**, *42*, 2135.

(28) Xia, Y.; Olsen, B. D.; Kornfield, J. A.; Grubbs, R. H. *J. Am. Chem. Soc* **2009**, *131*, 18525.

(29) Sheiko, S. S.; Möller, M. *Chem. Rev.* **2001**, *101*, 4099.

(30) Vlassopoulos, D.; Fytas, G.; Loppinet, B.; Isel, F.; Lutz, P.; Benoit, H. *Macromolecules* **2000**, *33*, 5960.

(31) Vayer, M.; Hillmyer, M. A.; Dirany, M.; Thevenin, G.; Erre, R.; Sinturel, C. *Thin Solid Films* **2010**, *518*, 3710.

(32) Zalusky, A. S.; Olayo-Valles, R.; Wolf, J. H.; Hillmyer, M. A. *J. Am. Chem. Soc.* **2002**, *124*, 12761.

(33) Hu, M.; Xia, Y.; McKenna, G. B.; Kornfield, J. A.; Grubbs, R. H. *Macromolecules* **2011**, *44*, 6935.

(34) Sveinbjörnsson, B. R.; Weitekamp, R. A.; Miyake, G. M.; Xia, Y.; Atwater, H. A.; Grubbs, R. H. *Proc. Natl. Acad. Sci. USA* **2012**, *109*, 14332.

(35) Troparevsky, M. C.; Sabau, A. S.; Lupini, A. R.; Zhang, Z. *Opt. Express* **2010**, *18*, 24715.

(36) Love, J. A.; Morgan, J. P.; Trnka, T. M.; Grubbs, R. H. *Angew. Chem. Int. Ed.* **2002**, *41*, 4035.